# Adsorption of oxygen on the paramagnetic defect centers in aluminophosphate molecular sieves

Sun Jin Kim, Myung Hoon Kim, Suk Bong Hong * and Young Sun Uh *

*Korea Institute of Science and Technology, PO Box 131, Cheongryang, Seoul 130-650, Korea*

Young-Sang Choi

*Department of Chemistry, Korea University, Seoul 136-650, Korea*

Received 12 November 1996; accepted 14 January 1997

Temperature-programmed desorption (TPD) and electron spin resonance (ESR) techniques have been employed to investigate the oxygen adsorbed on the paramagnetic defect centers in dehydroxylated $AlPO_4$-20, $AlPO_4$-11, $AlPO_4$-5, and VPI-5 molecular sieves. Two different adsorption sites are observed for the small-pore $AlPO_4$-20, where oxygen is entrapped within the intracrystalline voids generated during the calcination step, as well as within the $\beta$-cages. However, the unidimensional molecular sieves $AlPO_4$-11, $AlPO_4$-5, and VPI-5 have only one type of adsorption site within their inner pores. The apparent activation energies of desorption (12.0–21.7 kcal $mol^{-1}$) determined from the oxygen TPD results demonstrate that, as the pore size of the $AlPO_4$ molecular sieve is larger, the interaction between the adsorbed oxygen and the molecular sieve framework becomes weaker.

**Keywords:** oxygen adsorption, $AlPO_4$ molecular sieves, paramagnetic defects, TPD, ESR

## 1. Introduction

Several new families of molecular sieves have been reported over the last decade and include aluminophosphate ($AlPO_4$), silicoaluminophosphate (SAPO), metal-substituted aluminophosphate (MAPO), and gallophosphate ($GaPO_4$) molecular sieves [1–5]. The $AlPO_4$ molecular sieves were the first family of these phosphate-based molecular sieves to be discovered. Some of them have framework topologies which are analogous to those found in zeolites, while many are entirely novel structures. Due to the absence of Brønsted acid sites, however, little attention has been devoted to the development and characterization of $AlPO_4$ molecular sieves as catalysts and separation media.

There is a general acceptance that structural defects in zeolites and related materials can participate in determining their catalytic, ion exchange and adsorption properties [6]. Thus, detailed knowledge of the nature of these defects is of importance to understand the most essential aspects of molecular sieve chemistry. Very recently, we have found that dehydroxylation of $AlPO_4$ molecular sieves under a vacuum of $10^{-5}$ Torr at 773 K followed by adsorption of oxygen gives rise to the formation of the superoxide ion, $O_2^-$ [7]. This has been attributed to the electron transfer from the paramagnetic defect sites (F-type centers) in dehydroxylated $AlPO_4$ molecular sieves [8,9]. Therefore, it is expected that the unique electron-donating properties of paramagnetic defects generated in dehydroxylated $AlPO_4$ materials would receive much attention due to their potential use as novel catalytic centers for a variety of chemical reactions.

The purpose of this work is to investigate the interaction of the adsorbed oxygen with the paramagnetic defects in dehydroxylated $AlPO_4$ molecular sieves and to identify the location of adsorbed oxygen in these materials. Here we report the results obtained from oxygen temperature-programmed desorption (TPD) and electron spin resonance (ESR) measurements on a series of four $AlPO_4$ molecular sieves, namely $AlPO_4$-20, $AlPO_4$-11, $AlPO_4$-5, and VPI-5, which cover the range from small-pore to extra-large-pore systems. The TPD and ESR techniques have repeatedly attested to be very useful for studying the nature of oxygen adsorbates on a wide variety of solid surfaces including metal oxides and zeolites [10–12].

## 2. Experimental

$AlPO_4$-20, $AlPO_4$-11, and $AlPO_4$-5 were synthesized according to the procedures described in a Union Carbide patent [1]. $AlPO_4$-5 was also prepared in the presence of fluoride ions [13]. VPI-5 was synthesized by the procedures given elsewhere [14]. Crystallinity and phase purity of these molecular sieves were determined by X-ray powder diffraction (XRD) using a Rigaku D/Max-IIA diffractometer. All the samples were highly crystalline and showed no reflections other than those from the corresponding molecular sieve. The structural

* To whom correspondence should be addressed.

characteristics of the molecular sieves used in this study are given in table 1. As-synthesized molecular sieves were calcined under flowing oxygen at 873 K for 12–24 h, refluxed in water for 4 h, and then dried at room temperature for the reason described in our previous studies [7–9]. The nitrogen BET surface areas were measured on a Micromeritics ASAP 2000 analyzer.

The oxygen TPD was obtained on a Micromeritics TPD/TPR 2900 analyzer. Prior to the TPD measurements, a given amount of the samples was activated in flowing He at 773 K for 3 h, cooled to room temperature, and then exposed to pure oxygen (20 $cm^3$ $min^{-1}$) for 0.5 h. When necessary, the temperature of oxygen adsorption was varied from room temperature to 773 K. The thermogravimetric analyses (TGA) determined by a Dupont 950 thermogravimetric analyzer reveal that the four molecular sieves studied here have different water contents. Thus, the amount of the samples placed into the TPD cell was varied from 0.34 to 0.40 g in order to ensure that all samples have exactly the same weight after activation, i.e., 0.30 g. The treated samples were subsequently purged with helium at 373 K for 1 h to remove the physisorbed oxygen. These pretreatments were always carried out for fresh samples since repeated runs of TPD experiments can cause a serious decrease in the observed signal. Finally, the TPD experiments were performed in flowing helium (30 $cm^3$ $min^{-1}$) from 373 to 873 K with heating rates ranging from 5 to 30 K $min^{-1}$. In all present experiments the desorbed gas was identified to be oxygen alone by gas chromatography. The deconvolution of TPD signals, if required, was performed using the Origin Gaussian-fitting software.

ESR spectra were recorded at 77 K on a Bruker ER-200D spectrometer operating at X-band ($\sim$ 9.45 GHz) with 100 kHz field modulation. Before ESR measurements, approximately 30 mg of the samples were heated in a vacuum of $10^{-5}$ Torr at 773 K for 2 h, exposed to 10 Torr of oxygen at a given temperature for 0.5 h, and then evacuated in a vacuum of $10^{-5}$ Torr for 10 min at room temperature to remove the gas-phase oxygen. The microwave frequency was measured by an Anritsu MF76A microwave frequency counter and $g$ values are referenced to the resonant field of the 2,2-diphenyl-1-picrylhydrazyl (DPPH) radical at $g = 2.0036$.

Table 1
Structural information of $AlPO_4$ molecular sieves used in this study

| Material | Structure type | Ring size | Pore size (Å) |
|---|---|---|---|
| $AlPO_4$-20 | SOD | 6 | 2.2 |
| $AlPO_4$-11 | AEL | 10 | 3.9 × 6.3 |
| $AlPO_4$-5 | AFI | 12 | 7.3 |
| VPI-5 | VFI | 18 | 12.1 |

## 3. Results and discussion

Figure 1 shows the TPD curves for oxygen on $AlPO_4$ molecular sieves with four different structures which were purged with helium at 373 K after exposure to oxygen at room temperature. Figure 1a was obtained from the small pore $AlPO_4$-20. This TPD curve is characterized by two desorption peaks at 483 and 611 K, which indicates the presence of two different adsorption sites for oxygen. An unequivocal assignment to the low- and high-temperature desorption peaks observed in figure 1a will be given later. Unlike $AlPO_4$-20, on the other hand, the unidimensional molecular sieves $AlPO_4$-11, $AlPO_4$-5, and VPI-5 exhibit one desorption peak in the temperature region of 540–570 K, as seen in parts b–d in figure 1. This reveals that these three materials have only one type of oxygen adsorption sites. It is expected that no noticeable differences in the temperature at peak maximum ($T_M$) of desorption peaks may be observed, if the adsorption sites for oxygen are exclusively located on the outer surface of the $AlPO_4$ molecular sieve crystals. This is because the outer surface of the crystals is terminated by isolated Al-OH and P-OH groups that are independent of the structural features of the molecular sieves. However, the TPD curves in figure 1 clearly show that the $T_M$ values of the desorption peaks from $AlPO_4$ molecular sieves studied here are different. In general, the smaller pore size the molecular sieve has, the higher $T_M$ value of oxygen desorption it shows (see table 2). This suggests that the adsorption sites for oxygen are mainly located within the inner pores of the $AlPO_4$

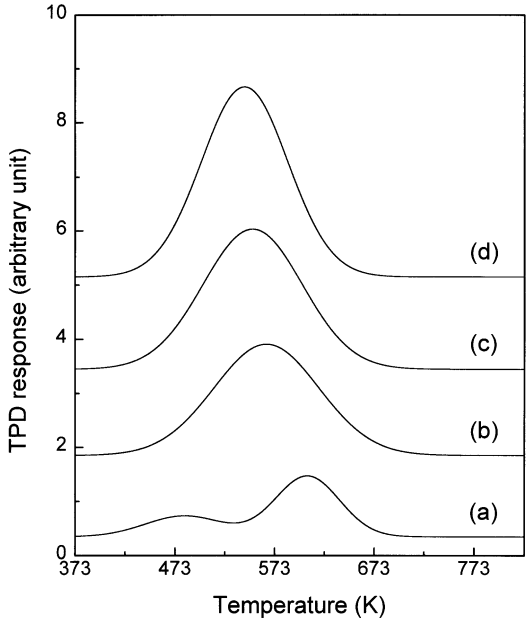


Figure 1. TPD curves for oxygen on $AlPO_4$ molecular sieves with different structures: (a) $AlPO_4$-20, (b) $AlPO_4$-11, (c) $AlPO_4$-5, and (d) VPI-5. Oxygen adsorption was performed at room temperature and the heating rate during desorption was maintained at 20 K $min^{-1}$.

Table 2
TPD results of oxygen adsorbed at room temperature on dehydroxylated $AlPO_4$ molecular sieves with different structures [a]

| Material | $T_M$ [b] (K) | Adsorption site | $V_d$ [c] ($cm^3\,g^{-1}$) | Concentration ($10^{18}\,g^{-1}$) | | $E_d^*$ [e] (kcal $mol^{-1}$) |
|---|---|---|---|---|---|---|
| | | | | $O_2$ | $O_2^-$ ion [d] | |
| | 483 | intracrystalline void | | | | 12.0 |
| $AlPO_4$-20 | | | 0.07 | 2.3 | 0.02 | |
| | 611 | $\beta$-cage | | | | 21.7 |
| $AlPO_4$-11 | 564 | 10-ring | 0.23 | 7.6 | 0.2 | 18.2 |
| $AlPO_4$-5 | 553 | 12-ring | 0.26 | 8.7 | 1.6 | 15.9 |
| VPI-5 | 543 | 18-ring | 0.46 | 15.0 | 2.9 | 14.3 |

[a] The heating rate was 20 K $min^{-1}$.
[b] The temperature at maximum of a desorption peak.
[c] The amount of desorbed oxygen.
[d] From ESR data in ref. [7].
[e] The apparent activation energy of desorption.

molecular sieve crystals rather than on their outer surface.

The $AlPO_4$ molecular sieves are built from alternating $AlO_4^-$ and $PO_4^+$ tetrahedra and thus are electrically neutral. This implies that they show no oxygen adsorption capacity at room temperature, if their framework is crystallographically perfect. However, it is rare for actual $AlPO_4$ molecular sieve crystals to have a perfect framework because structural defects are normally generated during the synthesis and/or post-synthesis steps [8,9]. Our recent investigations have demonstrated that dehydroxylation of structural defects in $AlPO_4$ molecular sieves at 773 K leads to the formation of paramagnetic defect centers which serve as adsorption sites for oxygen [8,9]. Therefore, we believe that the TPD peaks in figure 1 are mainly to be attributed to the oxygen adsorbed on the paramagnetic defects in $AlPO_4$ molecular sieves. To further ensure the speculation given above, we have synthesized $AlPO_4$-5 in the presence of fluoride ions and measured the oxygen TPD on this sample. This is because the amount of structural defects is greatly reduced by using $F^-$ ions as mineralizing agents in the synthesis of molecular sieves [15,16]. As expected, the intensity of the TPD signal observed from this $AlPO_4$-5 sample was found to be approximately three orders of magnitude weaker than that from the sample prepared by the conventional method. In addition, the fact that the same aluminum and phosphorus sources have been used in the synthesis of these two $AlPO_4$-5 samples led us to rule out the possibility that a small amount of paramagnetic impurities such as $Fe^{3+}$ or $Mn^{2+}$ ions present in $AlPO_4$ molecular sieves, possibly originated from the chemicals used in their synthesis, may be responsible for the oxygen adsorption.

To further characterize the two desorption peaks observed from the small-pore $AlPO_4$-20, the TPD measurements on this material have been performed after exposure to oxygen at different temperatures. The amounts of desorbed oxygen ($V_d$) for two desorption peaks were determined from the deconvolution of the TPD curves obtained and are plotted against the temperature of oxygen adsorption ($T_{ad}$) in figure 2. A specific $T_{ad}$ leading to the maximum $V_d$ is observed for both low- and high-temperature desorption peaks. However, notice that the low-temperature desorption peak shows the highest $V_d$ at $T_{ad} = 373$ K, while the high-temperature desorption peak reaches a maximum at a higher $T_{ad}$, i.e., 573 K. On the other hand, the sum of two desorption peaks possesses the highest $V_d$ value at $T_{ad} = 473$ K. These observations suggest that two different adsorption sites for oxygen in $AlPO_4$-20 are complementary to each other.

The framework of $AlPO_4$-20 is built from $\beta$-cages linked in a cubic array via single 4-rings (S4R), where

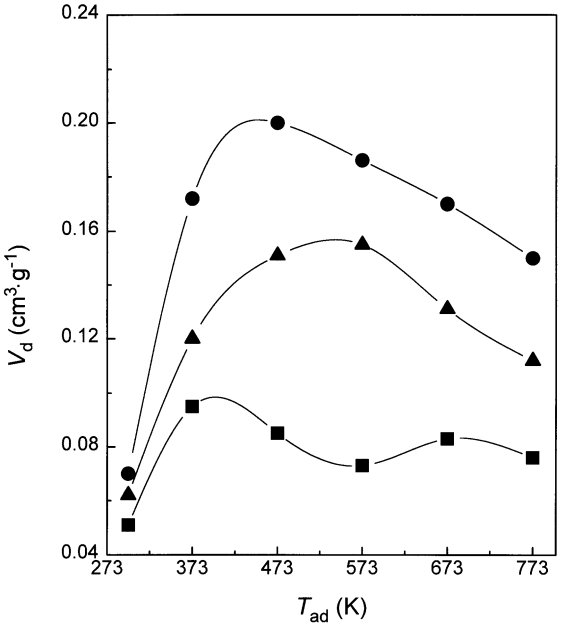


Figure 2. Changes in the amount of oxygen ($V_d$) adsorbed on $AlPO_4$-20 with respect to the adsorption temperature ($T_{ad}$). The solid squares and triangles represent the $V_d$ values of the low- and high-temperature desorption peaks in the TPD curves of $AlPO_4$-20, respectively. The solid circles indicates the total $V_d$ values.

adsorption of oxygen at room temperature is not possible [17]. Thus, if the $AlPO_4$-20 sample used in this study is crystallographically perfect, exposure of this small-pore material to oxygen at room temperature should give no detectable TPD peaks. As stated earlier, however, actual $AlPO_4$ molecular sieve crystals normally contain structural defects whose amount are dependent on the synthesis method and the manner of postsynthesis treatments. On the other hand, almost all $\beta$-cages of $AlPO_4$-20 retain one tetramethylammonium (TMA) ion used as the structure-directing agent in the synthesis of $AlPO_4$-20 after crystallization is complete [18]. Because the diameter ($\sim$ 6.4 Å) of TMA is much larger than that of the 6-ring opening (2.2 Å) of the $\beta$-cage, it is expected that the calcination step for the removal of TMA from a $\beta$-cage could lead to the partial collapse of the $AlPO_4$-20 framework due to the internal forces generated by the decomposition products of the TMA ion. This suggests that during the calcination step intracrystalline voids which are large enough to adsorb oxygen at room temperature are formed. If such is the case, the desorption process of oxygen within these intracrystalline voids during the TPD experiment should be to some extent hindered by the readsorption of the $\beta$-cages with elevating temperature. This is because oxygen can enter the $\beta$-cages at temperatures higher than 473 K [17]. Therefore, it is most likely that the low-temperature desorption peak in the TPD curve of figure 1a is due to oxygen released from intracrystalline voids generated by partial collapse of the $AlPO_4$-20 framework, while the high-temperature desorption peak is attributed to oxygen from the $\beta$-cages. In addition, it appears that the size of the intracrystalline voids in the $AlPO_4$-20 sample used here may be larger than that (12.1 Å) of the 18-ring channels of VPI-5, because the $T_M$ value (483 K) of the low-temperature desorption peak from $AlPO_4$-20 is lower than that (543 K) of the desorption peak from VPI-5.

Figure 3 shows the ESR spectra at 77 K of the $O_2^-$ ions generated by adsorption of oxygen at different temperatures on dehydroxylated $AlPO_4$-20. The $g_{zz}$ values of $O_2^-$ are measured at the maxima of the low-field peaks and reported to differ significantly according to their adsorption site [12]. As seen in figure 3a, the adsorption of oxygen to $AlPO_4$-20 at room temperature leads to the formation of $O_2^-$ ions with $g_{zz} = 2.0201$. The same result is obtained when $AlPO_4$-20 is exposed at temperature up to 473 K. However, the $O_2^-$ ions generated by adsorption at 573 K exhibit a new peak at $g_{zz} = 2.0230$ as well as the peak at $g_{zz} = 2.0201$ (figure 3b). In addition, only one peak is observed at $g_{zz} = 2.0230$ (figure 3c), when oxygen is introduced to $AlPO_4$-20 at 773 K. On the other hand, the ESR signals of the $O_2^-$ ions formed on $AlPO_4$-20 at room temperature were readily destroyed by exposure to 10 Torr of water vapor. However, the ions formed at 773 K showed no significant decrease in ESR intensity even after the sample storage at ambient conditions over 1 month. Therefore, it is most likely that the adsorption of

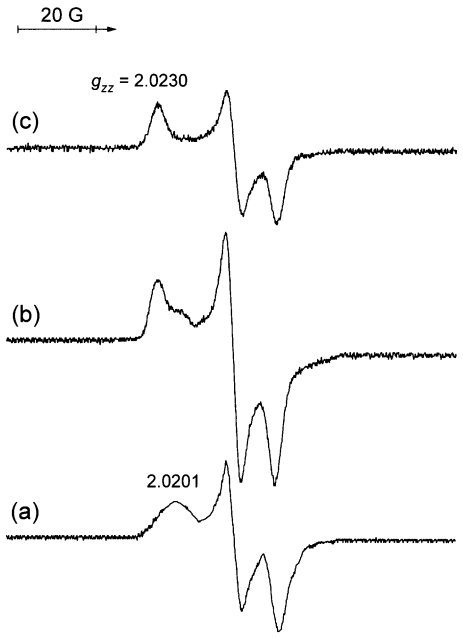


Figure 3. ESR spectra at 77 K developed after adsorption of oxygen on dehydroxylated $AlPO_4$-20 at (a) room temperature, (b) 573 K, and (c) 773 K.

oxygen at room temperature leads mainly to the desorption inside intracrystalline voids generated during the calcination step, while that at temperatures higher than 473 K results in the diffusion into the $\beta$-cages. This is consistent with the work of Imai and Habgood who investigated the effect of the temperature of oxygen adsorption on the location of $O_2^-$ in zeolite Na-Y [19].

The amounts of desorbed oxygen for $AlPO_4$ molecular sieves studied here were evaluated from their TPD peak areas and are listed in table 2. The spin concentrations of the $O_2^-$ formed in the corresponding molecular sieves are also compared in table 2. These data reveal that the larger pore size the molecular sieve has, the larger amount of desorbed oxygen it shows. Thus, the largest amount of desorbed oxygen (ca. $1.5 \times 10^{19}$ $g^{-1}$) is observed for the extra-large-pore VPI-5. However, the amount of desorbed oxygen for each $AlPO_4$ molecular sieve was found to be much larger than the spin concentrations of the $O_2^-$ formed in the same molecular sieve. This trend is more apparent to the small-pore $AlPO_4$-20, because of the encapsulation of oxygen within the $\beta$-cages. Therefore, it is most likely that only a small portion of oxygen molecules adsorbed on the paramagnetic defect sites in dehydroxylated $AlPO_4$ molecular sieves is changed into $O_2^-$ ions, although further study is necessary to understand this intriguing result.

On the other hand, the apparent activation energies ($E_d^*$) of oxygen desorption can be determined from the equations derived by Cvetanovic and Amenomiya [20]. Assuming that $E_d^*$ is independent of the amount of adsorbate and time, $E_d^*$ can be obtained using the following equations:

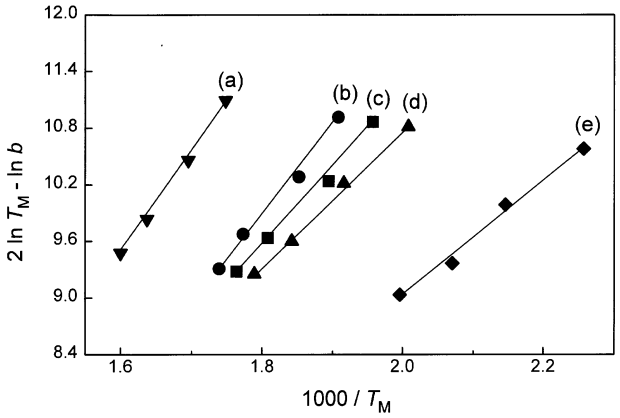


Figure 4. Plots of $(2\ln T_M - \ln b)$ versus $1/T_M$ for the TPD peaks of oxygen from (a) $AlPO_4$-20 ($\beta$-cages), (b) $AlPO_4$-11, (c) $AlPO_4$-5, (d) VPI-5, and (e) $AlPO_4$-20 (intracrystalline voids).

for first-order adsorption

$$2\ln T_M - \ln b = \frac{E_d^*}{RT_M} + \ln\frac{E_d^* V_m}{Rk_0}\,, \qquad (1)$$

for second-order adsorption

$$2\ln T_M - \ln b = \frac{E_d^*}{RT_M} + \ln\frac{E_d^* V_m}{Rk_0} - \ln V_m\theta_M\,. \qquad (2)$$

In these equations, $V_m$ is the amount of the adsorbate at full surface coverage, $b$ the heating rate, $\theta_M$ the surface coverage at peak maximum, $k_0$ the preexponential factor in the desorption rate expression, and $R$ is the gas constant. Thus, if the $T_M$ is measured as a function of $b$, $E_d^*$ can be determined from the plots of $(2\ln T_M - \ln b)$ versus $1/T_M$, without knowing the exact desorption order. Upon increasing from 5 to 30 K $min^{-1}$, all oxygen TPD peaks from $AlPO_4$ molecular sieves studied here exhibited a continuous increase in their $T_M$ values. However, their amounts of desorbed oxygen remained unchanged. All plots of $(2\ln T_M - \ln b)$ versus $1/T_M$ shown in figure 4 gave straight lines, which is in good agreement with the equations given above. From their slopes, the $E_d$ values were determined and are also listed in table 2. These data show that the oxygen adsorbates entrapped within the $\beta$-cages of $AlPO_4$-20 have the $E_d^*$ value of 21.7 kcal $mol^{-1}$, while those in the 18-ring channels of VPI-5 14.3 kcal $mol^{-1}$. Therefore, it is clear that the strength of the interaction between the adsorbed oxygen and the $AlPO_4$ framework is dependent on the pore size of the molecular sieve.

In conclusion, the overall results of this study demonstrate that the interaction of the adsorbed oxygen with the paramagnetic defect centers in aluminophosphate molecular sieves is different in the structure type of the molecular sieves. The apparent activation energy of desorption is found to become lower upon increasing the pore size of the molecular sieve where oxygen is adsorbed.

## Acknowledgement

Support of this work was provided by the Korea Institute of Science and Technology under the contract No. 2E14113.

## References

[1] S.T. Wilson, B.M. Lok, C.A. Messina, T.R. Cannan and E.M. Flanigen, US Patent 4,310,440 (1982).
[2] B.M. Lok, C.A. Messina, R.L. Patton, R.T. Gajek, T.R. Cannan and E.M. Flanigen, J. Am. Chem. Soc. 106 (1984) 6092.
[3] B.M. Lok, B.K. Marcus, L.D. Vail, E.M. Flanigen and S.T. Wilson, Eur. Patent Appl. 159,624 (1985).
[4] E.M. Flanigen, R.L. Patton and S.T. Wilson, Stud. Surf. Sci. Catal. 37 (1988) 137.
[5] E.M. Estermann, L.B. McCusker, Ch. Baerlocher, A. Merrouche and H. Kessler, Nature 352 (1991) 320.
[6] G. Engelhardt and D. Michel, *High-Resolution Solid State NMR of Silicates and Zeolites* (Wiley, New York, 1987).
[7] S.B. Hong, S.J. Kim, Y.S. Choi and Y.S. Uh, Stud. Surf. Sci. Catal. 105 (1997) 779.
[8] S.B. Hong, S.J. Kim and Y.S. Uh, J. Am. Chem. Soc. 118 (1996) 8102.
[9] S.B. Hong, S.J. Kim and Y.S. Uh, J. Phys. Chem. 100 (1996) 15923.
[10] M. Iwamoto, K. Maruyama, N. Yamazoe and T. Seiyama, J. Phys. Chem. 81 (1977) 622.
[11] M. Iwamoto, Y. Yoda, N. Yamazoe and T. Seiyama, J. Phys. Chem. 82 (1978) 2564.
[12] M. Che and A.J. Tench, Adv. Catal. 32 (1983) 1.
[13] J.L. Guth, H. Kessler, P. Caullet, J. Hazm, A. Merrouche and J. Patarin, in: *Proc. 9th Int. Zeolite Conf.*, Vol. 1, eds. R. von Ballmoos, J.B. Higgins and M.M.J. Treacy (Butterworth-Heinemann, Stoneham, 1993) pp. 215–212.
[14] M.E. Davis and D. Young, Stud. Surf. Sci. Catal. 60 (1991) 53.
[15] J.M. Chezeau, L. Delmotte, G.L. Guth and M. Soulard, Zeolites 9 (1989) 78.
[16] S.A. Axon and J. Klinowski, J. Appl. Catal. 81 (1992) 27.
[17] D.W. Breck, *Zeolite Molecular Sieves* (Wiley, New York, 1974).
[18] S.B. Hong, Microporous Mater. 4 (1995) 309.
[19] T. Imai and H.W. Habgood, J. Phys. Chem. 77 (1973) 925.
[20] R.J. Cvetanovic and Y. Amenomiya, Adv. Catal. 17 (1967) 103.